© 2022 This manuscript version is made available under the CC-BY-NC-ND 4.0 license
https://creativecommons.org/licenses/by-nc-nd/4.0/

The definitive publisher version is available online at
https://doi.org/10.1016/j.compbiomed.2022.105990

3D Brain Slice Classification and Feature Extraction Using Deformable Hierarchical Heuristic Model

Ramesh Sekaran[a], Ashok Kumar Munnangi[b], Ramachandran Manikandan[c], Amir H. Gandomi[d]

[a]*Department of Information Technology, Velagapudi Ramakrishna Siddhartha Engineering College, Vijayawada, Andhra Pradesh, India*
[b]*Department of Information Technology, Velagapudi Ramakrishna Siddhartha Engineering College, Vijayawada, Andhra Pradesh, India*
[c]*School of Computing, SASTRA Deemed University, Thanjavur, India.*
[d]*Faculty of Engineering & Information Systems, University of Technology Sydney, Sydney, Australia*

ARTICLE INFO

Keywords: Brain tumors,
MRI, 3D tumor, VOI,
DHHM-DDRN

Brain tumors are the most frequently occurring and severe type of cancer, with a life expectancy of only a few months in most advanced stages. As a result, planning the best course of therapy is critical to improve a patient's ability to fight cancer and their quality of life. Various imaging modalities, such as computed tomography (CT), magnetic resonance imaging (MRI) and ultrasound imaging, are commonly employed to assess a brain tumor. This research proposes a novel technique for extracting and classifying tumor features in 3D brain slice images. After input images are processed for noise removal, resizing, and smoothening, features of brain tumor are extracted using Volume of Interest (VOI). The extracted features are then classified using the Deformable Hierarchical Heuristic Model-Deep Deconvolutional Residual Network (DHHM-DDRN) based on surfaces, curves, and geometric patterns. Experimental results show that proposed approach obtained an accuracy of 95%, DSC of 83%, precision of 80%, recall of 85%, and F1 score of 55% for classifying brain cancer features.

1. Introduction

Brain tumors are produced by uncontrolled accumulation of cancerous tissue that can be implanted in various parts of the brain, which can drastically affect the body's responsive functioning. These tumors are considered one of the most dangerous and complicated types to diagnose and treat [2]. There are 2 sorts of tumors: benign as well as malignant tumors. While benign tumors are typically harmless, they can harm the brain's healthy tissue if they continue to grow then it turns into cancer cells. Brain cancer is defined by malignant tumors that grow within the brain [1]. A glioma refers to a tumor that develops in glial cells, which are the most abundant cells in the central nervous system that surround and insulate the neurons [3]. While meningiomas are usually benign, a small percentage of them are malignant and are more common in those aged 45 to 55 years. Over the past two decades, groundbreaking approaches and computer-aided methods for the segmentation of brain tumors have gradually emerged to better classify brain tumors.

Imaging technology is crucial in diagnosis and treatment of brain tumors. Doctors and researchers often utilize CT scans and MRIs to non-invasively examine the brain. Specifically, MRI images yield a huge volume of spatial brain structure information and the anatomy of soft tissue that are pertinent for medical diagnosis. The picture intensity of an MRI image affects four specifications: the density of protons (PD), which is governed by relative water molecule concentration; and T1, T2, and T2* relaxation, which indicate different local properties of individual protons [4].

Corresponding author: Amir H. Gandomi

E-mail address:gandomi@uts.edu.au

In cancer detection, treatment planning, and treatment outcome estimation, early detection via proper grading as well as classification of brain tumors is critical. Despite contemporary medical technological improvements, histological examination of biopsy specimens is still performed to diagnose, classify, and grade brain cancers [5]. To attain a final diagnosis, clinical examination as well as interpretation of imaging modalities like MRI or CT, followed by pathological tests, are routinely performed. However, this process is invasive, time-consuming, and prone to sampling errors. Using computer-aided and entirely automated detection as well as diagnosis systems to obtain rapid and accurate classification, it is possible for physicians and radiologists to make more accurate diagnoses in a shorter time. Precision labelling of MRI image pixels is needed for accurate MRI segmentation, which is used to detect contaminated tumor tissues and subsequently determine the optimal treatment and radiation therapy [6].

The process of this research is described as follows:

- To accurately predict brain tumors in 3D images, the proposed system performance was improved by adding additional class identifications to gain more data about type of brain tumor, enhance the quantity of training and test data, and thereby obtain more accurate results so that a better cancer prognosis can be made.

- The features in the region of the tumor processed brain image were extracted using Volume of Interest (VOI).

- The extracted image was classified using the Deformable Hierarchical Heuristic Model-based Deep Deconvolutional Residual Network (DHHM-DDRN)

- A parametric analysis was conducted to evaluate and compare the proposed technique with existing methods in terms of DSC, accuracy, precision, recall, and F1 score.

Organization of this article is as follows: section 2 presents related works; section 3 discusses proposed methodology; section 4 provides performance analysis; and section 5 concludes research.

2. Related Works

The segmentation pipeline in works using traditional machine learning approaches involves a preprocessing stage for feature extraction [7]. In [8], a semi-automatic approach was used to extract the tumor contour, from which 71 features were subsequently evaluated. Skull stripping is also a typical preparation stage in traditional discriminative techniques despite limitations, including parameter selection, the necessity for prior data about pictures, and long computation time [9]. Retrieved features are fed into a step of classification or segmentation. Another work [10] compared ANN (Artificial Neural Network) and SVM (Support Vector Machine) classifiers, which achieved accuracies of 75.6-94.9% and 79.3-91.7%, respectively. Similarly, [11] proposed an automatic brain tumor classification method based on 10 characteristics and a Back-Propagation Network as a classifier, obtaining a 95.3% accuracy. The use of fractal wavelet characteristics as input to a SOM (Self-Organizing Map) [12] resulted in an average precision of 90%. Instance-based learning is also used in tumor classification algorithms. For instance, [13] built a semi-automated system using a KNN classifier. To obtain a compression method called the region of interest (ROI), the authors [14] introduced a novel segmentation-based ACM, and those of [15] presented a region-based Active Contour Method (ACM) for segmentation that has good accuracy, sensitivity, and specificity. Furthermore, models based on brain regions are less sensitive to preliminary contours and are unable to segment images with inhomogeneous intensity. The author of [16] proposed a Geodesic Active Contour (GAC) model based on AC that increases over time depending on the image's underlying geometric measurements and uses an edge-based ACM to determine object boundaries [17]. Because only edge data are incorporated in the original GAC model, [18] developed a region-aided GAC method, which outperforms the conventional method, especially when dealing with pictures containing holes, weak edges, and noise [19]. In a competitive, unsupervised method of practice, the authors of [20] suggested a SOM approach that incorporates CNN with regularization and an altered SoftMax loss for segmenting images and obtained output images containing more segmented data than the input photos. In [21], the authors proposed a method using deep CNN that integrates segmentation as well as error correction portions, achieving a 2% higher accuracy than other methods and processing time of 40-50 ms [22]. Another study [23] suggested a brain tumor

detection as well as classification method in MR images, where a tumor section is first obtained from a brain image, then textural features of tumor are extracted using grey level co-occurrence matrix (GLCM) and classified utilizing a neuro-fuzzy classifier. In [24], the classification of brain MR images is based on FFNN classifiers and rough set theory. The authors of [25] proposed an SVM-based hybrid method for detecting brain tumors in MR images, which applies features of texture and intensity.

3. Proposed Model

This section discusses proposed design of brain tumor feature extraction and classification method using deformable models integrated with DL methods. Overall proposed architecture is given in Fig. 1. After input images are processed for noise removal, resizing, and smoothening, features of brain tumor are extracted using Volume of Interest (VOI). The extracted features are then classified using the Deformable Hierarchical Heuristic Model-Deep Deconvolutional Residual Network (DHHM-DDRN) based on surfaces, curves, and geometric patterns.

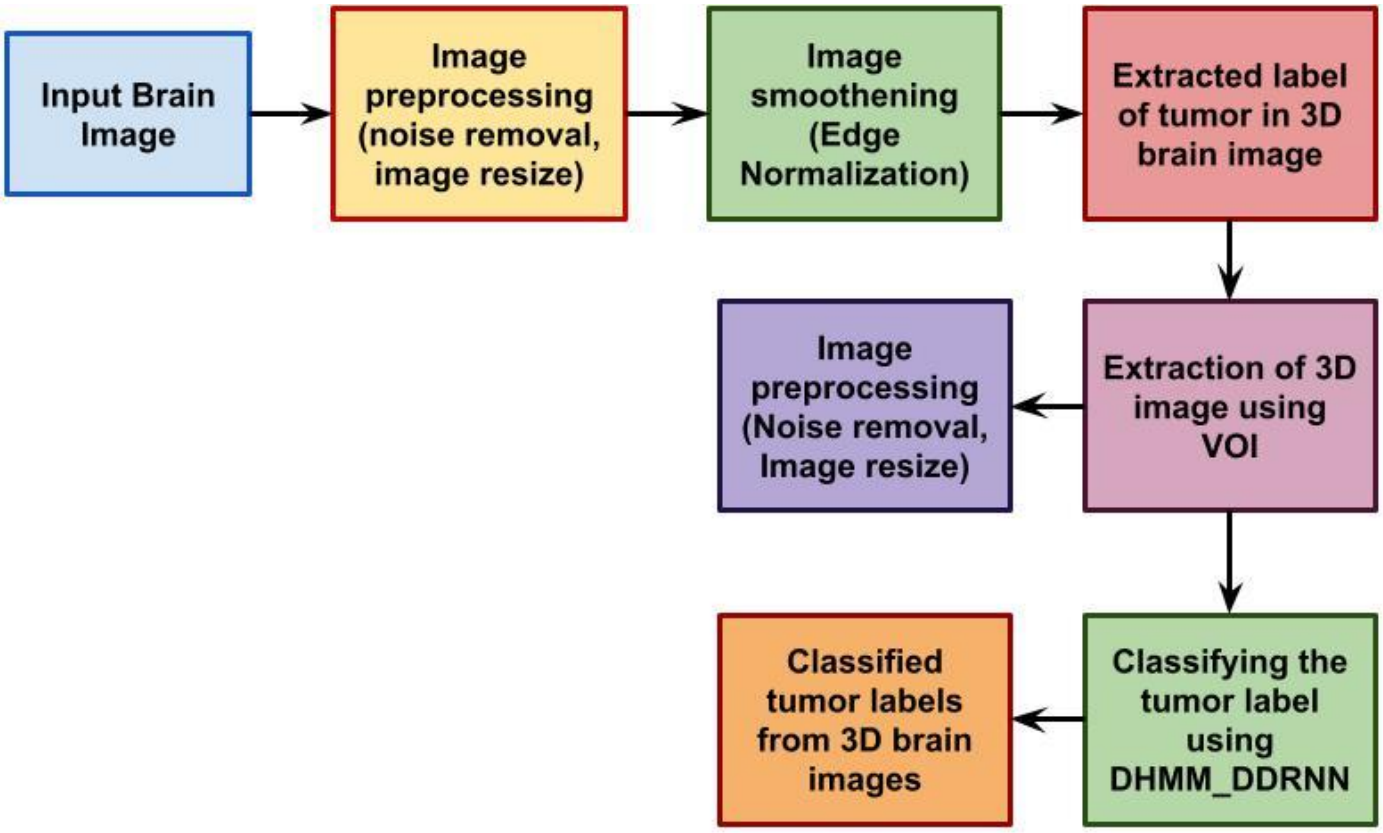

Fig. 1. Overall proposed architecture

3.1 Feature Extraction using Volume of Interest (VOI)

This section provides a full overview of the biological assumptions and derived equations. The proposed model contains two components, or two cell types, in a tumor: proliferating and non-dividing cells. Proliferating cells can either continue to segregate at a rate equal to the growth rate of tumor with t times cell p(D), which is termed proliferation probability, or shift to a non-dividing state at a rate equal to g(D). Non-dividing cells are removed from their initial position at a cell clearance rate of ηcl based on the proliferating tumor volume $V_T(t)$ and tumor growth rate λ(t). Tumor volume is derived using Eq. (1):

$$\frac{dV_T}{dt} = \lambda(t)\boldsymbol{V}_T$$
$$\frac{d\lambda}{dt} = -\theta\lambda(0)\lambda \qquad (1)$$

For τ_{rad} related to active radiation effect, ODEs are resolved by Eq. (2). i.e., in$t_R \leq t < t_R + \tau_{rad}$:

$$\frac{dV_T}{dt} = \lambda(t)p(D)\boldsymbol{V}_T - g(D)\boldsymbol{V}_T$$
$$\frac{dV_{ND}}{dt} = g(D)V_T - \eta_{cl}V_{ND}$$
$$\frac{d\lambda}{dt} = -\theta\lambda(0)\lambda \quad (2)$$

For $t > t_R + \tau_{rad}, V_T, V_{ND}$ and λ are results of corresponding ODEs given by Eq. (3):

$$\frac{dV_T}{dt} = \lambda(t)\boldsymbol{V}_T$$
$$\frac{d\boldsymbol{V}_{ND}}{dt} = -\boldsymbol{\eta}_{RI}\boldsymbol{V}_{ND}$$
$$\frac{d\lambda}{dt} = -\theta\lambda(0)\lambda \quad (3)$$

For LQ method, χ(D) is a function of α, and α/β is assumed by Eq. (4):

$$\chi(D) = \alpha D\left(1 + \frac{D}{\alpha/\beta}\right) \quad (4)$$

Parameters α, λ(0), θ, and ηcl indicate the best fit between design and experimental/clinical data for temporal changes in total tumor volume, i.e. sum of V_T *and* V_{ND} . V_T refers to total volume of cancerous cells, and T_{cc} is the time at which a malignant cell divides in the cell cycle. Some radiated cells stop proliferating and die when they are exposed to radiation, while other cells survive and continue to divide. V_{ND} is the volume of non-dividing cells, which separate from their original location. The following ODEs represent these processes:

$$\frac{dV_T}{dt} = f(V_T, V_v, D)V_T - g(D)V_T$$
$$\frac{dV_{ND}}{dt} = g(D)V_T - \eta_{cl}V_{ND} \quad (5)$$

where V_v is the vascular volume; and f and g are dependent on dose D. Consider function f, which has two elements, and is given by Eq. (6):

$$f(V_T, V_v, D) = \lambda(V_T, V_v)p(D) \quad (6)$$

The steps below must be completed for each cycle.

1) Reduce the image size to 140x90 pixels.

2) Using the mean shift approach, calculate an image segmentation. For a given x, where xi, i=1, n is a random set of n points inside a dataset. Mean shift process can be obtained by evaluating the mean shift vector m(x) via Eq. (7):

$$m(y_j) + y_j = \frac{\sum_{k=1}^{\infty} x_k g\left(\left\|\frac{y'_{i,j}-s_k}{h_k}\right\|^2\right) g\left(\left\|\frac{y'_{i,j}-F(s_k)}{h_r}\right\|^2\right)}{\sum_{i=1}^{\infty} g\left(\frac{y'_{ij}-s_k}{h_s}\|^2\right) g\left(\left\|\frac{y'_{i,j}-F(s_k)}{h_r}\right\|^2\right)} \quad (7)$$

Assuming y1 is the original value, the new concentrated x movement is evaluated using Eq. (8):

$$m(y_j) + y_j = \frac{\sum_{k=1}^{\infty} x_k g\left(\left\|\frac{y'_{i,j}-s_k}{h_k}\right\|^2\right) g\left(\left\|\frac{y'_{i,j}-F(s_k)}{h_r}\right\|^2\right)}{\sum_{i=1}^{\infty} g\left(\frac{y'_{ij}-s_k}{h_s}\|^2\right) g\left(\left\|\frac{y'_{i,j}-F(s_k)}{h_r}\right\|^2\right)} \quad (8)$$

3) Gray images are created from photos that pass the mean shift process.

4) Initial function φ0 is therefore described as follows:

$$\phi_0(x,y) = \begin{cases} -\rho & (x,y) \in \Omega_0 - \alpha\Omega_0 \\ 0 & (x,y) \in \Omega_0 \\ \rho & \Omega - \Omega_0 \end{cases} \quad (9)$$

where ρ > 0 is a constant.

5) Equation (9) computes early level set functions from an arbitrary region Ω0 in picture domain Ω.

For every patient P_{tcga}in TCGA data, the total cell number (TCN_{tcga}) that is considered proportional to tumor weight is given by Eq. (10):

$$\mathrm{TCN}_{tcga} = \alpha \frac{\text{tumor weight } (P_{\mathrm{tcga}})}{\frac{1}{\mathrm{K}}\sum_{\mathrm{all}P_{\mathrm{tega}}} \text{tumor weight } (P_{\mathrm{tcga}})} \quad (10)$$

In TCGA data, for K patients, the numbers of necrotic cells (N_{tcga}), cancer cells (C_{tcga}) and total immune cells (TIC_{tcga}) are evaluated by utilizing an erotic percentage (N_p) for each patient via Eq. (11):

$$\mathrm{N}_{\mathrm{tcga}} = \mathrm{TCN}_{tcga}\mathrm{N}_{\mathrm{p}}, \mathrm{C}_{\mathrm{tega}} = \frac{2}{3}\mathrm{TCN}_{tcga}(1 - \mathrm{N}_{\mathrm{p}}) \text{ and } \mathrm{TIC}_{\mathrm{tega}} = 0.5\mathrm{C}_{\mathrm{tcga}} \quad (11)$$

3.2 Deformable Hierarchical Heuristic Model-based Deconvolutional Residual Network (DHHM-DDRN)

Consider data $\{y_j\}$ with labels $\{z_j\}$as$\chi = \{(y_j, x_j) \mid y_j \in \Re^m, z_j \in \Re^n, j = 1, \ldots M]$, and DNN regulates a function $f_{DNN}: \Re^m \to \Re^n$. Neurons $x_j \in \Re$, 1layer of l neurons $x = (x_1, \ldots x_l)$, and ρ is the activation function. If a DNN has layers i = 0, . . .k, each of them has mi neurons given by Eq. (12):

$$x^{(i)} = \rho\left(\Theta^{(i-1)} \cdot x^{(i-1)} + a^{(i-1)}\right) (12)$$

Objective function $Min(F)$ is determined by Eq. (13):

$$F = \text{Min}\left[\text{Min}\left(\sum_{x=1}^{X} \text{Min}(f_1)\right) - \text{Min}(f_2) + \text{Min}(f_3)\right] \quad (13)$$

where f_1-f_3 are determined as follows,

$$f_1 = \text{Min}\left(\sum_{i=1}^{I}\sum_{y=1}^{Y}\sum_{z=1}^{z}\left(t_{ixyz}\right)\left(l_{ixyx}\right)\right)$$

$$f_2 = \text{Max}\left(\frac{I * X}{\sum_{i=1}^{l}\sum_{x=1}^{X}\sum_{y=1}^{Y}\sum_{z=1}^{z}\left(t_{ixyz}\right)\left(l_{lxyx}\right)}\right)$$

$$f_3 = \text{m}\left(\sum_{i=1}^{l}\sum_{y=1}^{Y}\sum_{z=1}^{z}\left(l_{lxyz}\right)\left(t_{ixyz}\right) - \sum_{i=1}^{l}\sum_{y=1}^{Y}\sum_{z=1}^{z}\left(l_{i(x+1)yz}\right)\left(t_{i(x+1)yz}\right)\right) \approx 0 \quad \forall M_x, x (14)$$

Decision variables and constraints are determined using Eq. (15):

$$\sum_{y=1}^{Y}\sum_{x=1}^{x}\sum_{z=1}^{z}\left(l_{ixyz}\right) = \sum_{y=1}^{Y}\sum_{x=1}^{X}\left(M_{ixy}\right)\left(To_{ixy}\right)\forall O_y \text{ of } J_i \text{ and } i, i = 1,2,,I \& y = 1,2,,Y$$

$$\sum_{x=1}^{X}\sum_{z=1}^{z} l_{ixyz} = \sum_{x=1}^{x}\left(M_{ixy}\right)\left(To_{Lxy}\right)\forall o_y \& J_i, i = 1,2,,I \& y = 1,2,,Y$$

$$\sum_{x=1}^{X}\left(M_{ixy}\right) = 1 \forall o_y \text{ of } J_i, \text{and } i, i = 1,2, I \& y = 1,2,,Y (15)$$

Consider an affine approximation to $f(\mathbf{X}) = \|\mathbf{Y} - \mathbf{H}_c\mathbf{X}\mathbf{H}_r^{\top}\|_{\text{F}}^2$ in (2) at $\mathbf{X}^{\ell}$, and following update rule in Eq. (16):

$$\mathbf{X}^{\ell+1} = \arg\min_{\mathbf{X}} f\left(\mathbf{X}^{\ell}\right) + \text{Tr}\left(\mathbf{X} - \mathbf{X}^{\ell}\right)^{\top}\nabla f\left(\mathbf{X}^{\ell}\right) + \frac{1}{2\eta}\|\mathbf{X} - \mathbf{X}^{\ell}\|_{\text{F}}^2 + \lambda\mathcal{G}(\mathbf{X}) \quad (16)$$

where$\|\mathbf{X} - \mathbf{X}^{\ell}\|_F^2$ is the proximal term; and X-Xl is the distal term. Using the definitions of proximal operators, the update for separable $\mathcal{G}(\mathbf{X})$ is written equivalently as Eq. (17):

$$\mathbf{X}^{\ell+1} = \mathcal{P}_{\nu}\left(\mathbf{X}^{\ell} - \eta\nabla f\left(\mathbf{X}^{\ell}\right)\right) \quad (17)$$

where $\mathcal{P}_{\nu}$ is the proximal operator for $\mathcal{G}$; and $\nu = \lambda\eta$ is the equal sign by Eq. (18):

$$\mathcal{G}(\mathbf{X}) = \| \mathbf{X} \|_1 \triangleq \sum_{i=1}^{M}\sum_{j=1}^{N}\left|X_{ij}\right| \quad (18)$$

The element-wise soft-thresholding (ST) function turns out to be the proximal operator in Eq. (19):

$$\mathcal{P}_{\nu}\left(X_{ij}\right) = \text{sgn}\left(X_{ij}\right)m\left\{\left|X_{ij}\right| - \nu, 0\right\} (19)$$

The traditional iterative shrinkage and thresholding processes are given by Eq. (20) and (21), respectively:

$$\nabla f(\mathbf{X}) = \mathbf{H}_c(\mathbf{H}_c\mathbf{X}\mathbf{H}_r - \mathbf{Y})\mathbf{H}_r \quad (20)$$

$$\mathbf{X}^{\ell+1} = \mathcal{P}_{\nu}\left(\mathbf{X}^{\ell} - \eta\mathbf{H}_c\mathbf{H}_c\mathbf{X}^{\ell}\mathbf{H}_r\mathbf{H}_r + \mathbf{C}\right) \quad (21)$$

An activation function is defined as a linear combination of K Gaussian derivatives, and the linear function [12] is defined in Eqns. (22) and (23):

$$\psi(u) = \sum_{k=1}^{K} c_k\phi_k(u), u \in \mathbb{R} \quad (22)$$

where

$$\phi_k(u) = u\exp\left(-\frac{(k-1)u^2}{2\tau^2}\right) \quad (23)$$

Training dataset D contains N examples $\left\{\left(\mathbf{Y}_q, \mathbf{X}_q\right)\right\}_{q=1}^{N}$, where $\mathbf{Y}_q = \mathbf{H}_c\mathbf{X}_q\mathbf{H}_r^{\top} + \boldsymbol{\xi}_q$. Random noise vectors $\boldsymbol{\xi}_q$ are considered to be independent and identically distributed. Let $\mathbf{c}^{\ell} \in \mathbb{R}^K, \ell = 1{:}\,L$ be coefficients of LET activation in layer `. Minimizing squared estimation error across all training examples yields optimal set of activation parameters c*, as follows:

$$J(\mathbf{c}) = \frac{1}{2}\sum_{q=1}^{N}\left\|\mathbf{X}_q^L\left(\mathbf{Y}_q, \mathbf{c}\right) - \mathbf{X}_q\right\|_2^2 \quad (24)$$

where the gradient of J(c) concerning c is required for optimization. Unless a very tiny step size is specified, optimization of J(c) utilizing GD tends to deviate. It should be pointed out that the Hessian does not have to be computed directly. To train the neural network parameters, only the Hessian-vector product is required. Therefore, the Hessian-free optimization (HFO) method was used in our training procedure, as shown in Eq. (25):

$$\tilde{J}(\mathbf{c}_i + \delta_c) = J(\mathbf{c}_i) + \delta_c^{\top}\mathbf{g}_i + \frac{1}{2}\delta_c^{\top}\mathbf{H}_i\delta_c \quad (25)$$

where $g_i = \nabla J(c)|_{c=c_i}$; $H_i = \nabla^2 J(c)|_{c=c_i}$; and δ_c is each iteration. The ideal search direction is determined by minimizing a regularized quadratic approximation, as follows:

$$\delta_c^* = \arg\min_{\delta_c} \tilde{J}(\mathbf{c}_i + \delta_c) + \gamma\|\delta_c\|_2^2$$

$$X_{t+1} = X_t + \text{Lévy}\ (d) \times X_t$$

$$\text{Lévy}(x) = 0.01 \times \frac{r_1 \times \sigma}{|r_2|^{\frac{1}{\beta}}}$$

$$\sigma = \left(\Gamma(1+\beta) \times \sin\left(\frac{\pi\beta}{2}\right)\right)^{1/\beta} \quad (26)$$

where d is dimension of position vectors. In [0,1], r1 and r2 are random numbers, β is constant, and Γ(x) = (x − 1). Fitness function is evaluated using Eqns. (27) and (28):

$$fit_i = \frac{1}{1+f_i} \quad (27)$$

$$fi = \frac{1}{n_j}\sum_{i=1}^{nj} d(X_j, C_i) \quad (28)$$

The level set function ϕ is a surface, whereby Ω⁺ is positive inside the region, Ω⁻ is a negative outside the region, and Ω⁰ is interface regions defined over an image space as follows:

$$\frac{\partial\varphi}{\partial t} = -F.|\nabla\varphi|, \varphi(x,y,t=0) = \pm d$$

$$F = -\alpha k \cdot g - \beta \cdot g - \lambda\nabla g \cdot \frac{\nabla\varphi}{|\nabla\varphi|}$$

$$g = \frac{1}{1 + |(\nabla G_\sigma) \otimes I(X)|^\beta}$$

$$G_\sigma(\varepsilon) = \frac{1}{\sqrt[\varepsilon]{\pi}} e^{-(\varepsilon/\sigma)2} (29)$$

The overall Proposed flowchart is shown in figure-2.

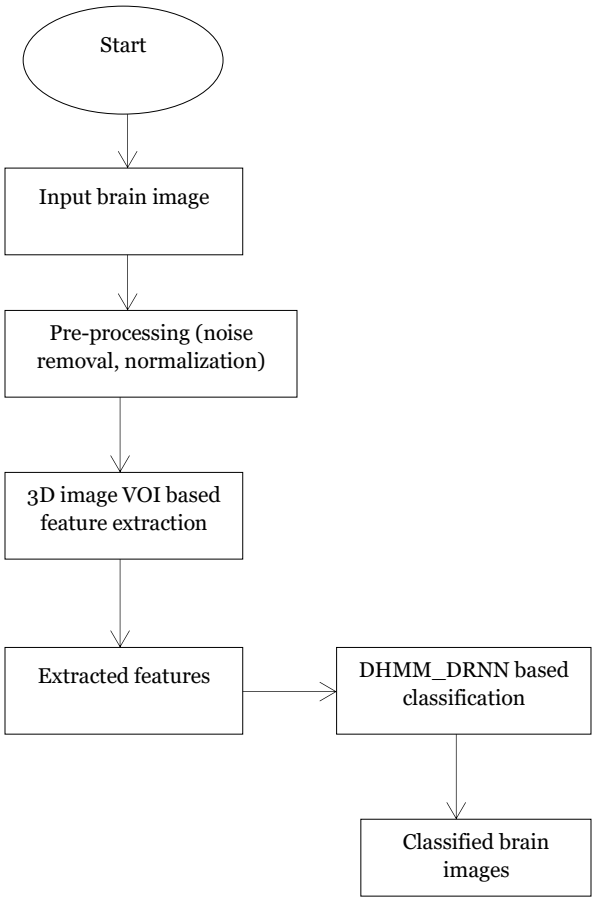

Figure-2 Overall Proposed Flow chart

VOI-DHHM-DDRN clusters to VOI algorithm

Input: D dataset consist of MRI brain images
Output: Best solution of the final cluster center $(C_{\text{list } j})j = 1,2,3,4$
Start step vectors ΔX_i
For $i = 1: S_N$
Start food source within boundary of the given dataset in random order
Calculate best potions of food sources by using ak-means technique
Direct dragonflies to food sources
End For
VOI-DHHM-DDRN Clusters to VOI Phase
Iteration = 0;
Do While
For $i = 1: n$
Evaluate fitness of every dragonfly
Renovate food source and enemy
EvaluateS, A, C, F, and E
Renovate neighboring radius
If

Renovate step vector (ΔX) and position vector X
Else
Renovate position vector
End if
Examine and precise new positions based on variables boundaries
For $i = 1{:}S_N$
Evaluate probability.
End For
For $i = 1{:}S_N$
If (rand () $< P_i$)
Evaluate new fitness of new food source chooses best food by utilizing a grasping.choose between old and new food sources.
i=i+1;
end if
output: Final clusters centers
end

4. Experimental procedure

Proposed feature extraction and classification technique was performed in Python with the following configurations: PC with Ubuntu, 8GB RAM, and Intel i3 processor CPU @1.70GHz, 64-bit operating system.

The following three datasets are a part of TCIA project's cancer imaging repository. Each case had FLAIR and T1-contrast-enhanced pictures**:**

RIDER dataset includes MRI-multi-sequence pictures from 19 glioblastoma patients (Grade IV) and 70,220 photos in total.

REMBRANDT (Repository of Molecular Brain Neoplasia Data) dataset includes MRI multi-sequence pictures of 130 patients with Grade II, III, and IV gliomas and 110,020 photos in total.

TCGA-LGG (Cancer Genome Atlas Low-Grade Glioma) dataset contains 199 patients with low-grade (I and II) gliomas are represented by 241,183 MRI scans.

5. Results

Table 1 Proposed feature extraction and classification of 3D brain slices

INPUT DATASET 3D BRAIN IMAGE	PROCESSED 3D BRAIN IMAGE	EXTRACTED FEATURE OF CANCER IN 3D	CLASSIFIED CANCER REGION OF 3D BRAIN IMAGE
RIDER DATASET	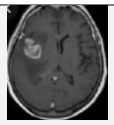	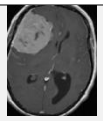	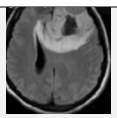
REMBRANDT	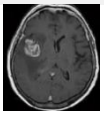	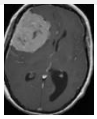	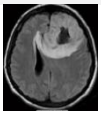
TCGA-LGG	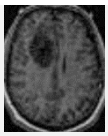	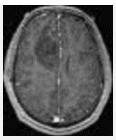	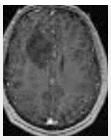

Table 1 shows the input brain cancer images achieved using the proposed volume-based region of cancer extraction and DHHM-DDRN-based classification.

Table 2 Comparative analysis of proposed and existing techniques

Parameters	ACM	GAC	VOI- DHHM-DDRN
Dice Similarity Coefficient (DSC)	77	79	83
Accuracy	83	91	95
Precision	65	71	80
Recall	80	82	85
F1 Score	43	51	55

Table 2 presents a comparative analysis of the proposed and existing (ACM and GAC) techniques based on DSC, accuracy, precision, recall, and F1 score. Results are illustrated in graph form in Figures 3, 4, 5, 6, and 7, respectively.

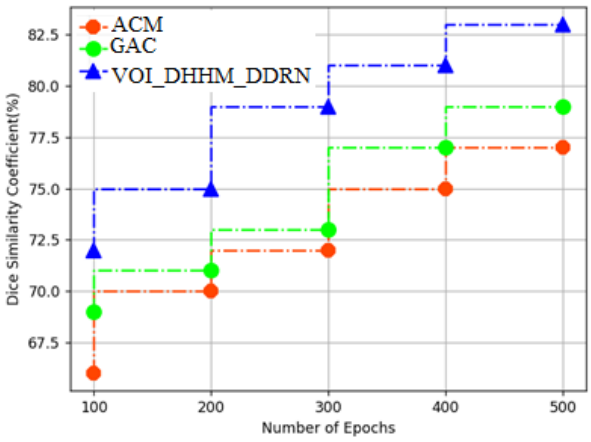

Fig. 3. DSC Comparison

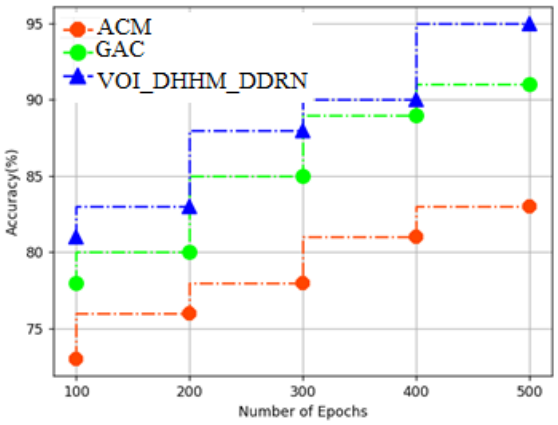

Fig. 4. Accuracy Comparison

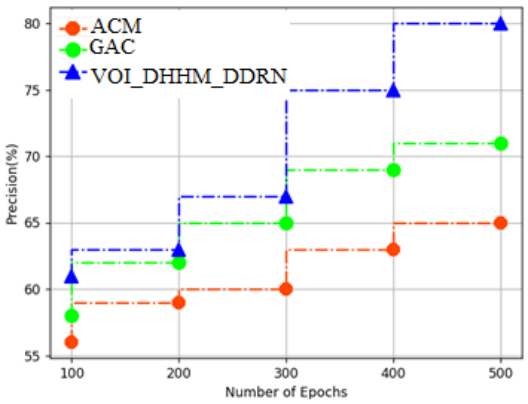

Fig. 5. Precision Comparison

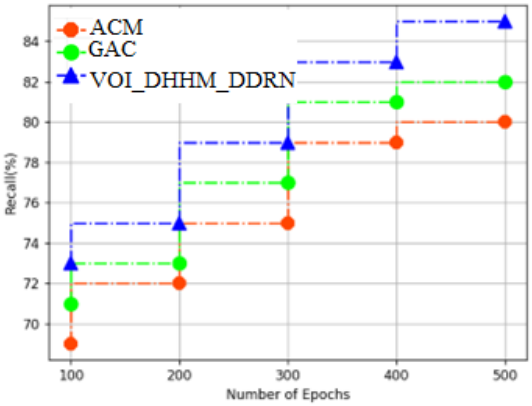

Fig. 6. Recall Comparison

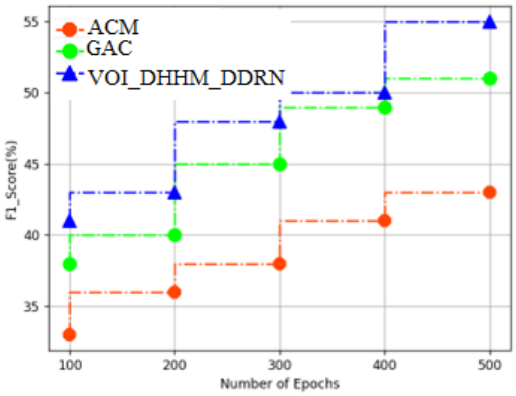

Fig. 7. F1 Score Comparison

Figures 7 presents the graphical representation of statistical metrics from Table II for a parametric comparison between proposed and existing method. It is apparent that proposed approach obtained optimal results with an accuracy of 95%, DSC of 83%, precision of 80%, recall of 85%, and F1 score of 55%.

6. Discussion:

Using MRI, radiologists may assess the brain. The presence of a tumour in brain is detected using the MRI technology. Human inspection is the traditional technique for finding tumours in MRI images. This process takes a long time. Large amounts of data are not appropriate. Additionally, noise introduced by operator interaction in the MRI can result in incorrect classification. Since there is a large number of MRI data to evaluate, automated systems are required because they are more efficient. Automated tumour diagnosis in MRI images is required since dealing with human life requires a high level of precision.

7. Conclusion

This research proposes a novel technique to extract the features and classify cancerous regions in 3D brain images. Specifically, the input images are initially processed for noise removal, resized, and smoothened. Then, features are extracted based on Volume of Interest (VOI) to accurately classify the tumor using the Deformable Hierarchical Heuristic Model-based Deep Deconvolutional Residual Network (DHHM-DDRN). In this study, we propose a four-stage classification scheme based on the extraction of brain tumor features utilizing the machine learning paradigm to support medical professionals. Due to the complexity of images and

dearth of anatomical methods that adequately represent various deformations in each component, medical image feature extraction is a difficult problem. A parametric analysis reveals that the reported method can achieve an accuracy of 95%, DSC of 83%, precision of 80%, recall of 85%, and F1 score of 55% in classifying features. It is suggested that future research use various optimization classifiers to increase the accuracy of such techniques by combining more efficient segmentation as well as extraction algorithms with real-time images, clinical cases, and a larger dataset that includes a variety of scenarios.

Ethics Approval

Not Applicable

Credit Authorship Contribution Statement

Ramesh Sekaran: Conceptualization, Methodology, Software, Validation, Formal Analysis, Writing – Original Draft, Visualization. **Ashok Kumar Munnangi:** Conceptualization, Investigation, Resources, Data Curation, Writing-Original Draft, Visualization. **Sivaram Rajeyyagari:** Software, Resources, Writing-Review & Editing. **Ramachandran Manikandan:** Formal Analysis, Supervision, Writing-Review & Editing. **Amir H. Gandomi:** Supervision, Writing-Review & Editing.

Declaration of competing interest

We declare that we have no known competing financial interests or personal relationships that could have appeared to influence the work reported in this paper.

Acknowledgements

Not Applicable.

References

[1] Badža, Milica M., and Marko Č. Barjaktarović. Classification of brain tumors from MRI images using a convolutional neural network. Applied Sciences 10.6 (2020) 1999.

[2] Noreen, Neelum, A deep learning model based on concatenation approach for the diagnosis of brain tumor. IEEE Access 8 (2020) 55135-55144.

[3] Tripathi, Sumit, Ashish Verma, and Neeraj Sharma. Automatic segmentation of brain tumour in MR images using an enhanced deep learning approach. Computer Methods in Biomechanics and Biomedical Engineering: Imaging & Visualization 9.2 (2021) 121-130.

[4] Díaz-Pernas, Francisco Javier, A deep learning approach for brain tumor classification and segmentation using a multiscale convolutional neural network. Healthcare. 9.2(2021).

[5] Sobhaninia, Zahra, Brain tumor segmentation by cascaded deep neural networks using multiple image scales. 2020 28th Iranian Conference on Electrical Engineering (ICEE), 2020.

[6] Landis, J. Richard, and Gary G. Koch. The measurement of observer agreement for categorical data. biometrics (1977) 159-174.

[7] Laukamp, Kai Roman, Automated meningioma segmentation in multiparametric MRI. Clinical Neuroradiology 31.2 (2021) 357-366.

[8] Khalil, Hassan A., 3D-MRI brain tumor detection model using modified version of level set segmentation based on dragonfly algorithm. Symmetry 12.8 (2020) 1256.

[9] Tungkasthan, Anucha, and WichianPremchaiswadi. Automatic region of interest detection in natural images. 15th WSEAS International Conference on Computers. hal. 2011.

[10] Watanabe, Yoichi, A mathematical model of tumor growth and its response to single irradiation. Theoretical Biology and Medical Modelling 13.1 (2016)1-20.

[11] Mohammad Mirzaei, Navid, A Mathematical Model of Breast Tumor Progression Based on Immune Infiltration. Journal of Personalized Medicine 11.10 (2021) 1031.

[12] Bhowmik, A., Bayesian Deep Deconvolutional Neural Networks, Second workshop on Bayesian Deep Learning (NIPS 2017), Long Beach, CA, USA.

[13] Yu, Heng, Zhiqing Zhou, and Qiming Wang. Deep learning assisted predict of lung cancer on computed tomography images using the adaptive hierarchical heuristic mathematical model. IEEE Access 8 (2020) 86400-86410.

[14] Singh, Ranbir, and B. Khan. Meta-hierarchical-heuristic-mathematical-model of loading problems in flexible manufacturing system for development of an intelligent approach. International Journal of Industrial Engineering Computations 7.2 (2016)177-190.

[15] Fakhry, Ahmed, Tao Zeng, and Shuiwang Ji. Residual deconvolutional networks for brain electron microscopy image segmentation. IEEE transactions on medical imaging 36.2 (2016) 447-456.
[16] Baid, Ujjwal, A novel approach for fully automatic intra-tumor segmentation with 3D U-Net architecture for gliomas. Frontiers in computational neuroscience 14 (2020):10.
[17] Azam, Muhammad Adeel, A review on multimodal medical image fusion: Compendious analysis of medical modalities, multimodal databases, fusion techniques and quality metrics.Computers in Biology and Medicine 144 (2022): 105253.
[18] Maharjan, Sunil, A novel enhanced softmax loss function for brain tumour detection using deep learning. Journal of neuroscience methods 330 (2020) 108520.
[19] Ataloglou, Dimitrios, Fast and precise hippocampus segmentation through deep convolutional neural network ensembles and transfer learning. Neuroinformatics 17.4 (2019) 563-582.
[20] Shehab, Mohammad, Machine learning in medical applications: A review of state-of-the-art methods. Computers in Biology and Medicine 145 (2022) 105458.
[21] Karayegen, Gökay, and Mehmet FeyziAksahin. Brain tumor prediction on MR images with semantic segmentation by using deep learning network and 3D imaging of tumor region. Biomedical Signal Processing and Control 66 (2021) 102458.
[22] Karayegen, Gökay, and Mehmet FeyziAksahin. Brain tumor prediction on MR images with semantic segmentation by using deep learning network and 3D imaging of tumor region. Biomedical Signal Processing and Control 66 (2021) 102458.
[23] Sadad, T., Rehman, A., Munir, A., Saba, T., Tariq, U., Ayesha, N., & Abbasi, R. (2021). Brain tumor detection and multi-classification using advanced deep learning techniques. *Microscopy Research and Technique*, *84*(6), 1296-1308.
[24] Ahmadi, M., DashtiAhangar, F., Astaraki, N., Abbasi, M., & Babaei, B. (2021). FWNNet: presentation of a new classifier of brain tumor diagnosis based on fuzzy logic and the wavelet-based neural network using machine-learning methods. *Computational Intelligence and Neuroscience*, *2021*.
[25] Arif, M., Ajesh, F., Shamsudheen, S., Geman, O., Izdrui, D., &Vicoveanu, D. (2022). Brain tumor detection and classification by MRI using biologically inspired orthogonal wavelet transform and deep learning techniques. *Journal of Healthcare Engineering*, *2022*.